Gondwana Research 54 (2018) 38–49

Contents lists available at ScienceDirect

Gondwana Research

journal homepage: www.elsevier.com/locate/gr

Imaging Precambrian lithospheric structure in Zambia using electromagnetic methods

Emily Sarafian [a,b,*,1], Rob L. Evans [b], Mohamed G. Abdelsalam [c], Estella Atekwana [c], Jimmy Elsenbeck [b], Alan G. Jones [d,2], Ezekiah Chikambwe [e]

[a] Massachusetts Institute of Technology-Woods Hole Oceanographic Institution Joint Program in Oceanography/Applied Ocean Science and Engineering, Woods Hole, MA 02543, USA
[b] Department of Geology and Geophysics, Woods Hole Oceanographic Institution, Woods Hole, MA 02543, USA
[c] Boone Pickens School of Geology, Oklahoma State University, Stillwater, OK 74078, USA
[d] Dublin Institute for Advanced Studies, Dublin, Ireland
[e] Geological Survey Department of Zambia, P.O. Box 50135, Lusaka, Zambia

ARTICLE INFO

Article history:
Received 19 March 2017
Received in revised form 8 August 2017
Accepted 14 September 2017
Available online 05 October 2017

Handling Editor: N. Rawlinson

Keywords:
Geology
Lithosphere
Aeromagnetics
Magnetotellurics
Zambia

ABSTRACT

The Precambrian geology of eastern Zambia and Malawi is highly complex due to multiple episodes of rifting and collision, particularly during the formation of Greater Gondwana as a product of the Neoproterozoic Pan-African Orogeny. The lithospheric structure and extent of known Precambrian tectonic entities of the region are poorly known as there have been to date few detailed geophysical studies to probe them. Herein, we present results from electromagnetic lithospheric imaging across Zambia into southern Malawi using the magnetotelluric method complemented by high-resolution aeromagnetic data of the upper crust in order to explore the extent and geometry of Precambrian structures in the region. We focus particularly on determining the extent of subcontinental lithospheric mantle (SCLM) beneath the Archean-Paleoproterozoic cratonic Bangweulu Block and the Mesoproterozoic-Neoproterozoic Irumide and Southern Irumide Orogenic Belts. We also focus on imaging the boundaries between these tectonic entities, particularly the boundary between the Irumide and Southern Irumide Belts. The thickest and most resistive lithosphere is found beneath the Bangweulu Block, as anticipated for stable cratonic lithosphere. Whereas the lithospheric thickness estimates beneath the Irumide Belt match those determined for other orogenic belts, the Southern Irumide Belt lithosphere is substantially thicker similar to that of the Bangweulu Block to the north. We interpret the thicker lithosphere beneath the Southern Irumide Belt as due to preservation of a cratonic nucleus (the pre-Mesoproterozoic Niassa Craton). A conductive mantle discontinuity is observed between the Irumide and Southern Irumide Belts directly beneath the Mwembeshi Shear Zone. We interpret this discontinuity as modified SCLM relating to a major suture zone. The lithospheric geometries determined from our study reveal tectonic features inferred from surficial studies and provide important details for the tectonothermal history of the region.

1. Introduction

The assembly of the Greater Gondwana supercontinent at ~600 Ma, following the breakup of Rodinia at ~830 Ma, marks an important tectonic event in Earth history (Stern, 2008). It is estimated that Neoproterozoic volcanism formed ~20% of the continental crust that is currently preserved in the form of orogenic belts circling older cratonic fragments that collided to create Greater Gondwana (Maruyama and Liou, 1998). Collision between different cratonic fragments at the end of the Neoproterozoic was accompanied by widespread remobilization (metacratonization) of either entire cratonic blocks or the cratonic margins (Abdelsalam et al., 2002; Liégeois et al., 2013).

There are substantial uncertainties in detailing the tectonic elements of the super-continent, especially the spatial distribution of cratonic fragments, the orogenic belts surrounding them, and the portions of the cratonic fragments that have been metacratonized. This is largely because many of the present-day fragments of Greater Gondwana are covered with Phanerozoic sedimentary rocks formed in large intra-continental sag basins (Artemieva and Mooney, 2001). Sub-continental lithospheric mantle (SCLM) thickness varies between tectonic elements, with typical estimates of a few tens of kilometers beneath active rifts to >250 km under certain cratons, though refertilization of old cratonic SCLM or cooling of young SCLM can cause delamination and thinning of the lithosphere (Begg et al., 2009; Khoza et al., 2013; Miensopust

* Corresponding author at: 266 Woods Hole Road, WHOI MS#22, Woods Hole, MA 02543, USA.
E-mail address: etursack@mit.edu (E. Sarafian).
[1] Now at Corning, Incorporated, Corning, NY, USA.
[2] Now at Complete MT Solutions Inc., Ottawa, Canada.

https://doi.org/10.1016/j.gr.2017.09.007
1342-937X/

et al., 2011). These lithospheric heterogeneities facilitated strain localization during Phanerozoic rifting (McConnell, 1972; Nyblade and Brazier, 2002), which further complicates the surface expression of the different Precambrian tectonic structures.

In Africa, which in many reconstructions is put as the heart of Greater Gondwana (Irving and Irving, 1982; Smith and Hallam, 1970), surface geological mapping, geochemical and geochronological studies together with low resolution seismic tomography (Abdelsalam et al., 2011; Begg et al., 2009; Deen et al., 2006; Lebedev et al., 2009; Pasyanos, 2010; Pasyanos and Nyblade, 2007; Ritsema and van Heijst, 2000; Shapiro and Ritzwoller, 2002) have resulted in establishing the extent of major cratons and orogenic belts of Greater Gondwana (Fig. 1A). However, identifying the geologic framework is particularly difficult in the region between the Bangweulu Block in northern Zambia and the Zimbabwe craton to the south (Fig. 1B) because few detailed studies of lithospheric structures exist in this area.

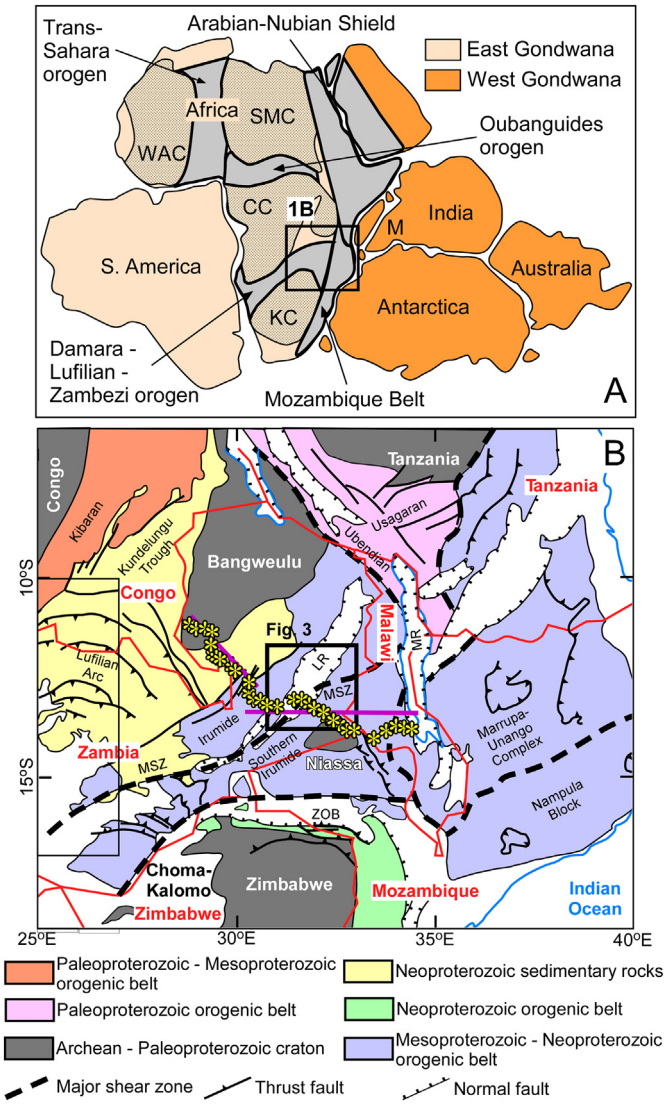

Fig. 1. (A) A reconstruction of Gondwana with the major tectonic elements of Africa identified from geological mapping, geochemical and geochronological studies, and seismic tomography. WAC: West African Craton; SMC: Saharan Metacraton; CC: Congo Craton; KC: Kalahari Craton. LR: Luangwa Rift. MR: Malawi Rift. The black box indicates the region of interest in this study as shown in panel B. (B) A simplified geological map showing the tectonic framework of Zambia and the surrounding region. Modified after Westerhof et al. (2008). Yellow stars show MT station locations. Dark pink traces show the Western Luangwa (WLUA) and Eastern Luangwa (ELUA) profiles, and their orientations, used during inverse modeling of MT data. Red lines show political boundaries. The black box highlights the area where high resolution aeromagnetic data was collected as shown in Fig. 3. MSZ: Mwembeshi Shear Zone; ZOB: Zambezi Orogenic Belt. (For interpretation of the references to colour in this figure legend, the reader is referred to the web version of this article.)

In this paper, we present results from two-dimensional (2D) isotropic inversion of a NW-SE magnetotelluric (MT) regional profile collected across Zambia and southern Malawi (Figs. 1B and 2A). Stations in Zambia are labeled "W" and "E" in Fig. 2B whereas stations in Malawi are labeled "M" in the same figure. This regional profile crosses major Precambrian entities including the Bangweulu Block, the Irumide and Southern Irumide Orogenic Belts (separated by the Mwembeshi Shear Zone), and the foreland sedimentary rocks portion of the Lufilian Orogenic Belt (referred to here as the Lufilian Foreland Basin) (Fig. 1B). Our MT profile crosses the NE-trending Paleozoic - Mesozoic (Permian to Triassic) Karoo-age Luangwa Rift, the southwestern part of which follows the Mwembeshi Shear Zone whereas its northeastern part extends within the Irumide Belt. The profile extends to the Malawi Rift at the eastern margin of the Southern Irumide Belt (Figs. 1B and 2A).

MT is a natural-source electromagnetic imaging method, and maps the lateral and vertical subsurface resistivity structure, and is sensitive to variations in temperature, composition, and interconnected conductors, such as fluid, melt, or metals. As a result, MT is a powerful tool to investigate lithospheric-scale structures (Evans et al., 2011; Jones, 1999; Khoza et al., 2013; Miensopust et al., 2011; Muller et al., 2009). In addition to the mantle-probing MT data, we also use high-resolution aeromagnetic data over the Mwembeshi Shear Zone and surrounding Irumide and Southern Irumide Belts, provided by the Geological Survey Department of Zambia, to unveil the upper crustal structure (Fig. 3). The combination of electrical models derived from our MT data and high-resolution aeromagnetic data allows us to reveal the extent of the SCLM and improve our understanding of the Precambrian structures in the region – those obvious in surface geology, and those oblivious to surface geology as they are buried at depth. In particular, our work facilitates delineation between stable cratonic blocks with thick SCLM from those with thinned SCLM, possibly due to partial delamination and regional metacratonization, and provides detailed images of the lithospheric boundaries (suture zones) between different Precambrian entities. Our work also touches upon the possible influence of the Precambrian structures on the evolution of the Karoo rifts represented by the Luangwa Rift, although it is not our primary focus. Before discussing the data, results, and geological implications of our study, we first define the key terms of craton and metacratons, and then briefly discuss the geological background and previous geophysical studies of the region of study.

2. Cratons and metacratons

Cratons primarily occupy the interior of continental plates. They are Archean to Paleoproterozoic in age, and have been tectonically stable for long periods of time, possibly since the time of their formation, albeit with frequent modification in many cases due to influx of metasomatizing fluids. Such long-lasting stability is attributed to the presence of a thick, cold and mostly anhydrous SCLM beneath the cratonic continental crust (Black and Liégeois, 1993; Peslier et al., 2010). The thick, depleted nature of the SCLM makes it sufficiently buoyant to be isolated from the convecting mantle surrounding the cratonic keel (Arndt et al., 2009; Hirth et al., 2000; Pollack, 1986). In Africa, examples of stable cratons (at least their interior portions) include the composite West African Craton, the composite Congo Craton, and the composite Kalahari Craton (Fig. 1A).

To explain the nature of the lithosphere in northern Africa, Abdelsalam et al. (2002) introduced the term Saharan 'metacraton' as 'a craton that has been remobilized during an orogenic event, but that is still recognizable predominantly through its rheological, geochronological, and isotopic characteristics'. In this definition, the prefix 'meta' abbreviates the word 'metamorphosis' in the general sense of the term and is not in the restricted geological meaning of 'metamorphism'. Abdelsalam et al. (2011) proposed that partial SCLM delamination or

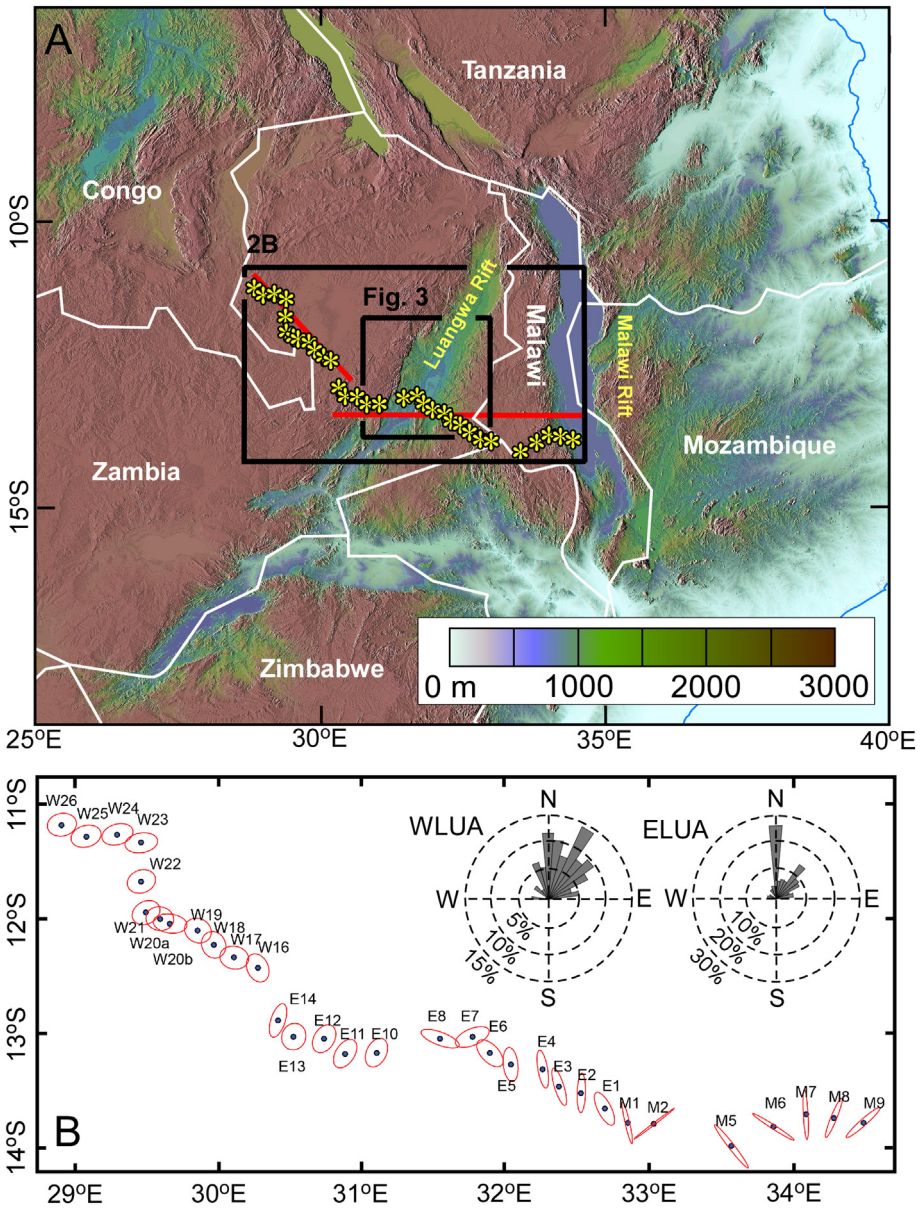

Fig. 2. (A) Shuttle Radar Topography Mission (SRTM) Digital Elevation Model (DEM) courtesy NASA/JPL-Caltech of the region of Fig. 1B. Yellow stars indicate MT station locations. Stations traverse from eastern Zambia into southern Malawi. Red traces show the Western Luangwa (WLUA) and Eastern Luangwa (ELUA) profiles, and their orientations, used during inverse modeling of MT data. The black box highlights the area where high resolution aeromagnetic data was collected as shown in Fig. 3. White lines show political boundaries. (B) The MT phase tensor for each station determined at a period of 89 s. Stations labeled with a "W" lie on the WLUA profile. Stations labeled with an "E" lie on the ELUA profile within Zambia. Stations labeled with a "M" lie on the ELUA profile within Malawi. (For interpretation of the references to colour in this figure legend, the reader is referred to the web version of this article.)

convective removal of the cratonic root is the responsible mechanism for metacratonization. It has been suggested that metacratonization can also occur locally due to plate collision along the margins of cratons or the development of lithospheric-scale shear zones in the interior of cratons (De Waele et al., 2006b; Liégeois et al., 2013; Liégeois et al., 2003). For example, De Waele et al. (2006b) and Liégeois et al. (2013) used the presence of Paleoproterozoic-Neoproterozoic high-K granitoids that intrude the Irumide Orogenic Belt in Zambia as evidence of multiple stages of metacratonization of the southern margin of the Archean-Paleoproterozoic cratonic Bangweulu Block. They determined that the Irumide represented the southern continuation of the Bangweulu Block before being metacratonized.

Liégeois et al. (2003) proposed that the development of major N-trending lithospheric-scale shear zones in the once intact cratonic block of the Hoggar in Algeria led to planar delamination of the SCLM resulting in zonal metacratonization leading to the present configuration of the Hoggar as interleaving N-trending slivers of cratons and metacratons. This notion is further supported by MT imaging of part of the Tuareg Shield in southern Algeria, where sub-vertical crustal-scale conductors were observed coincident with the surface exposure of major shear zones (Bouzid et al., 2015).

Metacratonization is not the only process resulting in modification of the SCLM beneath cratons. Studies focusing on mantle xenoliths and xenocrystals, as well as MT studies, have shown that metasomatic processes can significantly modify the SCLM of cratons (Griffin et al., 2009; Begg et al., 2009; Selway, 2015). For example, Selway (2015) found from a MT study that the SCLM of the Tanzanian Craton is significantly more conductive than the Mozambique Orogenic Belt, despite the low geotherm and the faster S-wave velocity that characterize the craton. Selway (2015) explained the high conductivity of the SCLM of the Tanzanian Craton as due to high water content from metasomatic fluids.

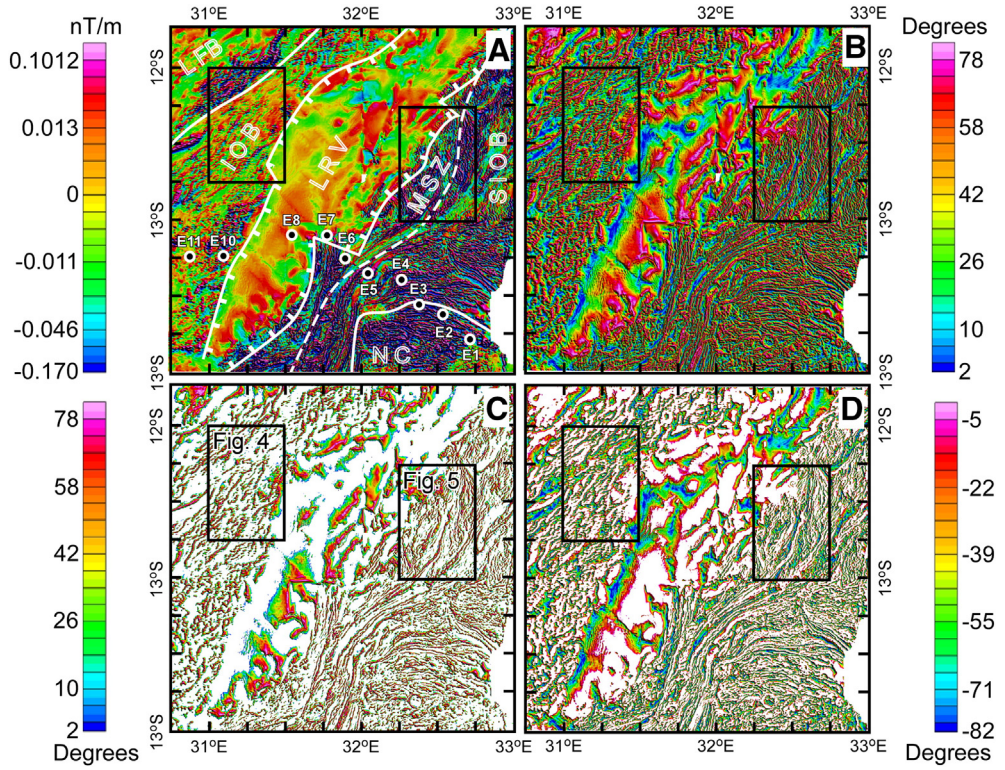

Fig. 3. Aeromagnetic images showing the shallow crustal structures of portions of the Lufilian Foreland Basin (LFB), Irumide Orogenic Belt (IOB), Southern Irumide Orogenic Belt (SIOB), Niassa Craton (NC), Mwembeshi Shear Zone (MSZ), and Luangwa Rift Valley (LRV). (A) Vertical derivative map from the total magnetic field data. (B) Tilt derivative image derived from the ratio of the vertical and horizontal derivatives of the total magnetic field. (C) Positive tilt image. (D) Negative tilt image.

3. Geological setting

The lithospheric structure beneath eastern Zambia and southern Malawi is poorly constrained, but surface geology indicates that the tectonic elements traversed by our MT profile include the Archean-Paleoproterozoic Bangweulu Block (De Waele et al., 2006b), the Mesoproterozoic-Neoproterozoic Irumide and Southern Irumide Orogenic Belts (separated by the Mwembeshi Shear Zone), and the Neoproterozoic Lufilian Foreland Basin (De Waele et al., 2009; Johnson et al., 2006; Johnson et al., 2005; Westerhof et al., 2008). In some publications, the central part of the Southern Irumide Orogenic Belt is shown to be occupied by a cratonic nucleus, referred to as the Niassa Craton (Fig. 1B) (Andreoli, 1984). The Precambrian geology of our study area is overprinted by two separate Phanerozoic rifting events: the Paleozoic – Mesozoic Karoo rift (represented by the Luangwa Rift) and the Cenozoic East African Rift System (represented by the Malawi Rift) (Figs. 1B and 2A). These Phanerozoic structures are not our primary focus, but will later briefly discuss their possible modification of the Precambrian lithospheric structures that we imaged.

3.1. The Bangweulu Cratonic Block

The Bangweulu Block is a cratonic block to the SW of the Tanzania Craton that underlies most of northern Zambia (Fig. 1B). Early studies of the Bangweulu Block identified a crystalline basement of schist, metavolcanics, granitoids, and gneisses overlain by Neoproterozoic sedimentary cover. The metavolcanics and gneisses were dated to be Paleoproterozoic in age (1.84–1.72 Ga). However, the presence of 2.73 Ga granites suggests that at least a portion of the Bangweulu Block is Neoarchean in age (Andersen and Unrug, 1984; Begg et al., 2009; Boniface and Schenk, 2012; De Waele et al., 2006b).

The Bangweulu Block is thus thought to be a Neoarchean microcontinent that was strongly affected by Paleoproterozoic tectonic events (Begg et al., 2009; De Waele et al., 2006b). Prior to the Neoproteozoic Pan-African Orogeny, an ocean basin and magmatic arc separated the Tanzania Craton from the Bangweulu Block. Collision of the Bangweulu Block and Tanzania Craton at ca. 1.95 Ga formed the Ubendian Orogenic Belt (Fig. 1B) (Begg et al., 2009; Boniface and Schenk, 2012; Lenoir et al., 1994). Subsequently, at ca. 1.8 Ga, the Tanzania-Bangweulu Craton collided with the Congo Craton forming the composite Congo-Tanzania-Bangweulu Craton (CC in Fig. 1A). Towards the end of the formation of Greater Gondwana, the ocean basin separating the Congo-Tanzania-Bangweulu Craton and Kalahari Craton (the northern part of which is referred to as the Zimbabwe Craton; Fig. 1A and B) was subducted and the two cratons collided along the Damara-Lufilian-Zambezi Orogenic Belt (Fig. 1A) in the late Neoproterozoic – early Cambrian Damara-Lufilian-Zambezi Orogeny (Johnson et al., 2005).

3.2. The Irumide and Southern Irumide Belt

The Irumide and Southern Irumide Belts are thick-skinned fold and thrust belts (folding and thrusting involve both basement and cover) that lie to the SE of the Bangweulu Block and Lufilian Foreland Basin (Fig. 1) (Ackermann, 1950; Ackermann, 1960; Daly, 1986). Detailed geochronological studies by De Waele et al. (2003, 2006a, 2006b, 2009) and Johnson et al. (2005, 2006) established four lithotectonic units for the Irumide Belt. (1) Paleoproterozoic (2.05–1.96 Ga) with minor Archean (2.7 Ga) crystalline granitic gneissic basement complex. (2) Paleoproterozoic (1.94–1.66 Ga) metasedimentary rocks (quartzites and meta-pelites. (3) Early Mesoproterozoic (1.66–1.52 Ga) granitoids. (4) Late Mesoproterozoic to early Neoproterozoic (1.05–0.95 Ga) granitoids. Similar geochemical and isotopic signatures of different granitoid pulses in the southern edge of the Bangweulu Block and the Irumide

Belt (2.05–1.95; 1.88–1.85; 1.65–1.55; and 1.05–0.95 Ga) and lack of juvenile subduction-related rocks in the Irumide Belt may indicate that the Irumide Belt is the southern margin of the Bangweulu Block that was metacratonized at 2.0, 1.85; 1.6 and 1.0 Ga (De Waele et al., 2006a).

Johnson et al. (2005, 2006) determined that the Irumide Belt and Southern Irumide Belt experienced different magmatic histories reflected by the lack of early Mesoproterozoic granitoids in the Southern Irumide Belt. They concluded that the crust underlying the Southern Irumide Belt is not the southward continuation of the crust of the Irumide Belt. Rather, it represents allochthonous continental arc terranes that collided with the Irumide Belt during the Mesoproterozoic Irumide Orogeny and was later reworked during the late Neoproterozoic – early Cambrian Damara-Lufilian-Zambezi Orogeny (Fig. 1A and B). Johnson et al. (2006) suggested that the Irumide Belt and the Southern Irumide Belt are separated by a suture zone, possibly represented by the ENE-trending Mwembeshi Shear Zone (also referred to as the Mwembeshi dislocation, MSZ, Fig. 1B) that has segments buried beneath the Paleozoic-Mesozoic Luangwa Rift Zone. Johnson et al. (2007) go further and suggest that this suture zone formed as a result of a young, hot oceanic slab subducting beneath the Irumide Belt during the Irumide Orogeny. Additionally, the Southern Irumide Belt is thought to contain an elusive cratonic nucleus known as the Niassa Craton (Fig. 1B) (Andreoli, 1984; Daly, 1986). Based on U/Pb geochronological data from zircons, this cratonic nucleus is believed to be a coherent lithospheric unit approximately Archean in age and covered by Paleoproterozoic sedimentary rocks and is therefore considered "lost" (De Waele et al., 2006a, 2009). In this regard, De Waele et al. (2009) considered the region to the south of the Irumide Belt to be the Niassa Craton.

3.3. The Lufilian Foreland Basin

The Lufilian Foreland Basin, as defined in this text, is associated with the Neoproterozoic Lufilian Orogenic Belt (Zientek et al., 2014). The Lufilian Belt is a NE-pointing triangular-shaped outcrop of variably-deformed sedimentary and volcanic rocks that lies between the Bangweulu Block in the northeast, the Kibaran orogenic belt in the northwest, and the Irumide Belt in the southeast. It is suggested to be part of a network of orogenic belts in central Africa that includes the Zambezi and Damara Belts (Fig. 1B) (Begg et al., 2009; Katongo et al., 2004; Porada and Berhorst, 2000). The origin of the belt is thought to be a Neoproterozoic rift basin, referred to as the Katanga basin that extended in the present location of southeastern Congo and northern Zambia around the margin of the Congo Craton during the fragmentation of Rodinia ca. 880 Ma (Batumike et al., 2006; Cailteux et al., 2005; Master et al., 2005). This was followed by subsequent collision of the Congo-Tanzania-Bangweulu Craton and Kalahari Craton at ca. 550 Ma during the Lufilian Orogeny, which is considered part of the Pan African Orogeny (Porada and Berhorst, 2000). This Neoproterozoic Pan-African Orogeny resulted in the deformation of the Katanga basin and the formation of the Lufilian Arc to the southwest as a top-to-the-northeast fold and thrust belt (Kampunzu and Cailteux, 1999; Porada and Berhorst, 2000; Selley et al., 2005; Zientek et al., 2014). It is also possible that this resulted in the formation of relatively undeformed foreland basins including the Kundelungu tough northeast of the Bangweulu Block and another trough to the southeast of it that is traversed by our MT profile (Fig. 1B; Zientek et al., 2014).

Building on the studies by Kampunzu and Cailteux (1999), Porada and Berhorst (2000) and Selley et al. (2005), Zientek et al. (2014) divided the Lufilian Belt into a number of tectono-stratigraphic units resting on the Paleoproterozoic (2.05 Ga–1.80 Ga) basement of the Bangweulu Block and the Mesoproterozoic (1.3 Ga–1.0 Ga) basement of the Irumide and Kibaran belts. Zientek et al. (2014) identified the oldest unit within the Lufilian Belt to a Neoproterozoic (0.76 Ga–0.73 Ga) mafic volcanic rock province, which is overlain by felsic province constituting granites and rhyolites, that were intruded and extruded during the late Neoproterozoic and early Cambrian (0.56 Ga and 0.53 Ga). Further, Zientek et al. (2014) divided the top-to-the-northeast fold and thrust belt of the Lufilian Belt, that is dominated by clastic and carbonate sedimentary rock into, from southwest to northeast, the Katanga High (where the basement was thrust northeast-ward atop the sedimentary rock), followed by the Synclinorial Belt, followed by the Domes Region, followed by the External Fold and Thrust Belt, and then the flat-lying sedimentary rocks of the foreland basin. Our MT profile traverses the Lufilian Foreland Basin flat-lying sedimentary rocks in the southeast margin of the Bangweulu Block (Fig. 1B).

4. Previous geophysical studies

Few geophysical studies have focused directly on our study region resulting in poor resolution imaging of the lithospheric structures and uncertainties in the delineation of tectonic elements. In recent seismic work, O'Donnell et al. (2013) resolved the lithospheric shear-velocity structure in the region around the Tanzania Craton, including Zambia and Malawi, using a large teleseismic dataset from the AfricaArray East African stations. They found a high-velocity region in eastern Zambia coincident with the known Bangweulu Block, as well as low velocity regions in the northern and southern areas of the Malawi Rift thought to be related to active rifting along the Western Branch of the East African Rift System (EARS). At depths < 100 km, the Bangweulu Block is the dominant high-velocity feature in Zambia. At greater depths, the dominant seismically fast feature migrates to the southeast into the Southern Irumide Belt. The deep, high velocity region in the Southern Irumide Belt is interpreted to be a subsurface extension of the Archean Bangweulu Block, with upwards of 200 km thick lithosphere (O'Donnell et al., 2013), which may be the expression of the inferred Niassa Craton. However, the lateral and particularly vertical resolution of this model is low within Zambia and decreases with depth limiting the interpretation of lithospheric structures in the region and calling into question the true extent of the high velocity anomaly within the Southern Irumide Belt.

5. Data and analysis

5.1. Aeromagnetic data and analysis

The aeromagnetic data used in this study were acquired by Geometrics Inc. for the Geological Survey Department of Zambia between 1973 and 1976 with a mean terrain clearance of 150 m and mean line spacing of 800 m–1000 m in the N-S direction. The International Geomagnetic Reference Field (IGRF) (Thébault et al., 2015) was removed from the data. We applied the vertical derivative (vertical gradient) filter to the total magnetic field data to highlight the trends of the Precambrian regional structures in the Irumide and Southern Irumide Orogenic Belts, the Mwembeshi Shear Zone, and the southeastern Lufilian Foreland Basin (Figs. 3A–5A). Vertical derivative maps accentuate short-wavelength anomalies while attenuating the long-wavelengths such that breaks, discontinuities, and rock fabric are highlighted.

Additionally, to enhance the ability to interpret the Precambrian structures, we also applied the tilt derivative filter developed by Miller and Singh (1994), Thurston and Smith (1997), Verduzco et al. (2004), Smith and Salem (2005), and Salem et al. (2007). We derived the tilt derivative images by computing the ratio between the vertical derivative and horizontal derivative of the total field magnetic data (Figs. 3B–5B). In these images, the tilt angle defines the contacts between geological materials that have alternating high and low magnetic susceptibilities (Salem et al., 2007). The calculated tilt angles range between +90° and −90° with the angle values with (+) sign the steeper features (in this case the high frequency features in Precambrian fabric) (Figs. 3C–5C). The angle values with (−) sign indicate the shallower structural features (Figs. 3D–5D). The tilt derivative has its zero values close to the edges of the body and is positive over the source and can resolve

subtle deeper structures (Miller and Singh, 1994). Therefore, the spatial images of the tilt map can be used to determine the approximate horizontal and lateral extent of features such as faults, geologic contacts, and edges of basins and uplifts.

5.2. Magnetotelluric data and analysis

MT data were collected in a profile of 36 broadband MT sites from northern Zambia into southern Malawi in 2012, with usable data provided from 32 stations (Figs. 1B and 2A). Stations were spaced ~20 km apart in a roughly NW-SE trending profile, but were limited to existing roads and tracks, causing minor variability in station spacing. The MT traverse extends from the Bangweulu Flats in northwestern Zambia (underlain by the Bangweulu Block and the Lufilian Foreland Basin) across the Muchinga Mountains (where the Irumide Orogenic Belt is exposed on the northwestern footwall of the Luangwa Rift Valley), the Luangwa Rift Valley, and the flexural zone of the Luangwa Rift Valley (where the Mwembeshi Shear Zone and the Southern Irumide Orogenic Belt are exposed) to the Malawi Rift (Fig. 6A). Five component time series magnetotelluric data were recorded by Phoenix Geophysics V5 Systems for 2–3 days over a period range of ~0.003 s (384 Hz) up to several thousand seconds, yielding high quality responses that facilitate good resolution of lithospheric structures (Fig. S1). At each site were measured the naturally occurring time-varying two horizontal electric and three magnetic field variations in orthogonal components: Hx, Hy, Hz, and Ex and Ey.

The MT time series were first processed by applying the robust techniques of Jones and Jödicke (1984) (Method 6 in Jones et al., 1989) in the Phoenix Geophysics SSMT2000 processing software, and converted to apparent resistivities and phases. The code employs the Least Trimmed Squares robust approach independently developed by Rousseeuw (1984). Sites deployed simultaneously served as remote references during processing to reduce bias in the calculated response. The dimensionality of the data with depth was qualitatively determined using phase tensor analysis (Caldwell et al., 2004) at all period bands and at four different period bands (Figs. 2B and S2). The shortest periods sampling shallow depths indicate a 3D structure, and longer periods (deeper depths) suggest a less complex 2D mantle structure. Periods that indicated 3D structure were not included in our 2D inversions. The dominant geo-electric strike direction for each profile segment was determined using Groom-Bailey galvanic distortion decomposition (Groom and Bailey, 1989) using the multi-site, multi-frequency STRIKE software package (McNeice and Jones, 2001). MT responses from sites along the western end of the profile were decomposed to a dominant geo-electric azimuth of 30 E of N. Sites along the eastern end of the profile had a dominant strike perpendicular to the acquisition geometry (Fig. 2B).

Based on the strike and dimensionality analysis, the array was split into two profile segments in order to perform 2D inverse modeling of the electrical structure: the western Luangwa profile (WLUA) and the eastern Luangwa profile (ELUA) (Fig. 2A). Prior to inversion, scattered data points with high error bars in apparent resistivity, phase, and tipper were removed in order to ensure that unreliable points were not influencing the inversions. In some cases at some sites, this resulted in the complete removal of one of the modes of response. Both profile segments were inverted for 2D isotropic electrical structure along profiles perpendicular to the geo-electric strike roughly following the acquisition profiles (30 W of N for WLUA and E-W for ELUA). Electrical models were generated by simultaneously inverting transverse electric (TE) and transverse magnetic (TM) apparent resistivities and phases, as well as vertical magnetic components (tipper), using a 2D regularized inversion scheme (Rodi and Mackie, 2001), as implemented in the WinGLink software package. Static shifts in the apparent resistivities of both modes were inverted for during modeling. Topography was not considered in inversions. Assigned error floors were 10% and 15% on TM and TE apparent resistivity, respectively, 5% on phases, and an absolute error floor of 0.1 for tipper. Smoothing parameters in the inversion algorithm controlled overall model smoothness (tau, the Tikhonov trade-off parameter), and smoothness of horizontal and vertical features (alpha and beta) to obtain the smoothest model that minimized data misfit and produce continuous horizontal features without unnecessary structure. Tau values were varied between 100 and 0.01 to produce an L-curve in order to assess overfitting and over smoothing of the data (Fig. S3). Based on our variations of the smoothing parameters, the final tau, alpha, and beta values used for these data were 1.0, 1.5, and 1.7 respectively. The preferred 2D isotropic resistivity models for the WLUA and ELUA profiles were derived from an initial 100 Ω m half-space starting model. Features produced during inversions were tested for sensitivity to ensure that the data required all features present in the final models. After hundreds of iterations with many restarts, the final normalized root-mean-squared (nRMS) misfit for the WLUA and ELUA 2D electrical models (Fig. 6C) were 1.81 and 1.73, respectively. Total nRMS misfit for each station, as well as the misfit of the two modes and tipper, is plotted above the resistivity models. Misfit is greatest in the easternmost sites along both the WLUA and ELUA profile, with the highest misfits concentrated in the stations close to the Malawi Rift (Fig. 6B).

6. Results

6.1. Aeromagnetic results

Interpretation of the aeromagnetic maps yields the following features: The Luangwa Rift Valley is represented by broad magnetic anomalies indicative of sedimentary fill of the rift. The Precambrian fabric is represented by short wavelength magnetic anomalies defined by alternation of low and high amplitudes in the vertical derivative image (Fig. 3A), and alternation of low and high degrees in the tilt (Fig. 3B), positive tilt (Fig. 3C) and negative tilt images (Fig. 3D). The Irumide Orogenic Belt is dominated by roughly NE-trending magnetic fabric (Fig. 3A–D) that is obvious in the positive and negative tilt images (Fig. 3C and D). The Lufilian Foreland Basin, away from its contact with the Irumide Orogenic Belt, is characterized by the presence of long wavelength magnetic signature similar to that found in the Luangwa Rift Zone (Fig. 3A–D). This might be due to the presence of the flat-lying foreland sedimentary rocks that overlay the Bangweulu Block. The boundary between the Lufilian Foreland Basin and the Irumide Orogenic Belts is marked by a sharp contrast in the amplitudes of the vertical derivative aeromagnetic image (Fig. 4A). This suggests that this boundary separates domains of different composition. To the southwest, the Mwembeshi Shear Zone is represented by a sharp magnetic lineament obvious in all aeromagnetic images (Fig. 3A–D). This lineament juxtaposes a western domain dominated by a more northerly magnetic fabric with a domain in the east dominated by NE-trending fabric. It is possible that the difference in the orientation of the magnetic fabric is due to the presence of the Irumide Orogenic Belt west of the shear zone and the Southern Irumide Orogenic Belt to the east of it. To the east of the Mwembeshi Shear Zone, the magnetic fabric changes into E-W trending (Fig. 3A–D), and this is where the northern edge of the Niassa Craton is mapped (Fig. 1B). In the northeast, the magnetic fabric suggests the presence of terrains of complex folding on both sides of the Mwembeshi Shear Zone (Fig. 5A–D).

6.2. Magnetotelluric results

6.2.1. Western Luangwa (WLUA) profile

The electrical model of the WLUA profile (Fig. 6C, left) shows the following features:

(1) A highly resistive feature (>10^3 Ω m) throughout the Bangweulu Block and Lufilian Foreland Basin. In the central portion of the profile the resistive feature extends to depths of ~250 km.

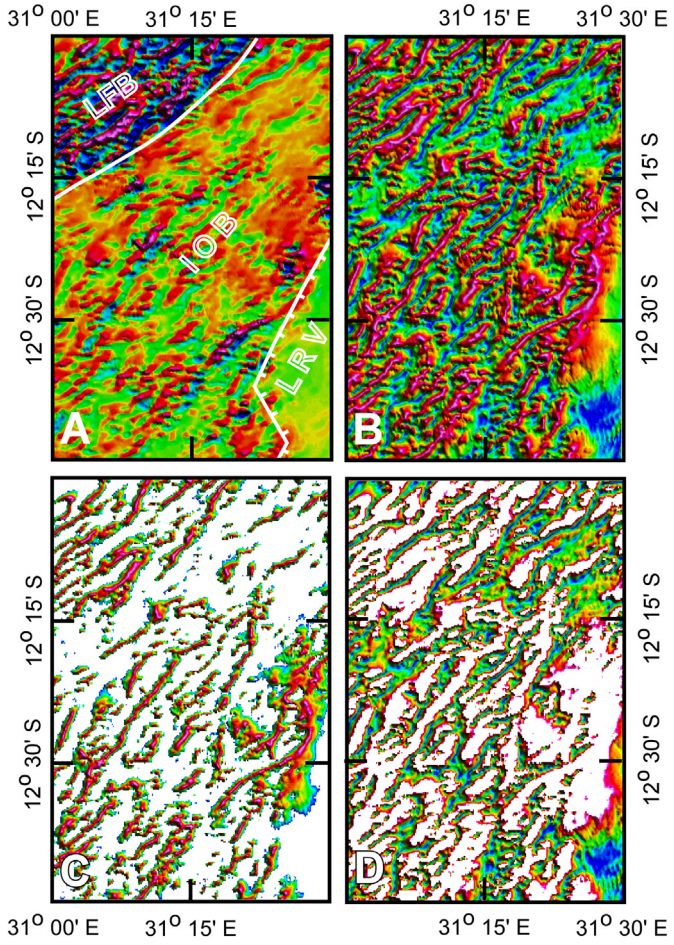

Fig. 4. (A) The vertical derivative map generated from the total magnetic field data, (B) tilt derivative image derived from the ratio of the vertical and horizontal derivatives of the total magnetic field, (C) positive tilt image, and (D) negative tilt image of portions of the Lufilian Foreland Basin (LFB), Irumide Orogenic Belt (IOB), and Luangwa Rift Velley (LRV). See Fig. 3 for location.

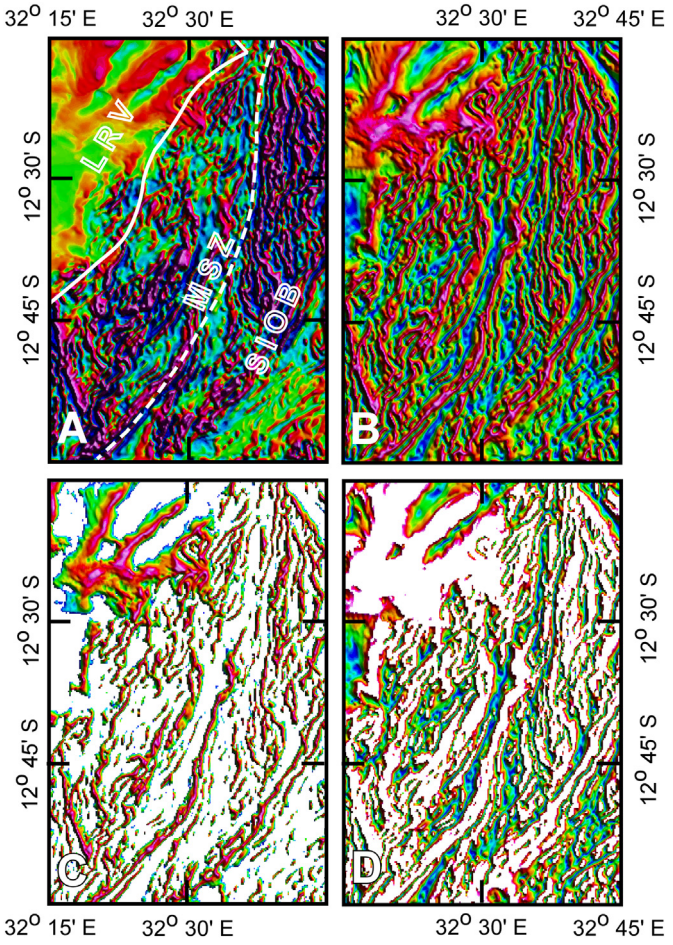

Fig. 5. (A) The vertical derivative map generated from the total magnetic field data, (B) tilt derivative image derived from the ratio of the vertical and horizontal derivatives of the total magnetic field, (C) positive tilt image, and (D) negative tilt image of portions of the Luangwa Rift Valley (LRV), Mwembeshi Shear Zone (MBZ), and Southern Irumide Orogenic Belt (SIOB). See Fig. 3 for location.

(2) Deep asthenospheric resistivities beneath the region have values of <300 Ω m.

In order to test the resolution and robustness of the observed resistive feature in the WLUA model, we manually edited the model and then ran a forward model (Fig. S1A), as well as additional inversion sequences. Due to static shifts affecting the apparent resistivity responses, we compare the phase responses of the forward model to the observed phases, and critique the misfit at individual sites. Differences in phase between the forward model and the observed data, as well as the final model and observed data, were calculated in pseudosections (Figs. S4 and S5).

Our tests of the observed resistive feature involved:

(1) Decreasing the resistivity at depth below the Bangweulu Block and Lufilian Foreland Basin.

Thinning the resistive root beneath the Bangweulu Block and Lufilian Foreland Basin to 180 km resulted in poor fit to the TE (6° to 10°) and TM (3° to >10°) phases at the longest periods in all sites (Fig. S5). The preferred model TE and TM fit phases at all periods generally to within 2° in the region of the Bangweulu Flats (Fig. S4). The systematic misfit, particularly in the TM phases, indicates that a feature is required by data but is not being modeled if the resistivity below the Bangweulu Flats is decreased. Thus, the resistive root is a robust feature.

6.2.2. Eastern Luangwa (ELUA) profile

The electrical model of the ELUA profile (Fig. 6C, right) shows the following features:

(1) Resistive mantle (>10^3 Ω m) that is ~150 km thick below the Irumide Belt on the western end of the profile.
(2) A highly conductive crust and broad conductive feature (<100 Ω m) present throughout the mantle beneath sites E6–E8 within the Mwembeshi Shear Zone and dipping to the west beneath sites E10–E14.
(3) A resistive anomaly (~10^3 Ω m) beneath the conductive crust of the Southern Irumide Belt that persists to depths of 250 km.
(4) A highly conductive crust (~1 Ω m) in the eastern end of the profile in Malawi.
(5) Crustal resistivities are much lower throughout the ELUA profile than the WLUA profile.
(6) Deep asthenospheric resistivities beneath the region that have values of <300 Ω m.

Similar tests were conducted to investigate the extent of observed features in the ELUA model (Figs. S1B; S6–S10). Our tests of each feature involved:

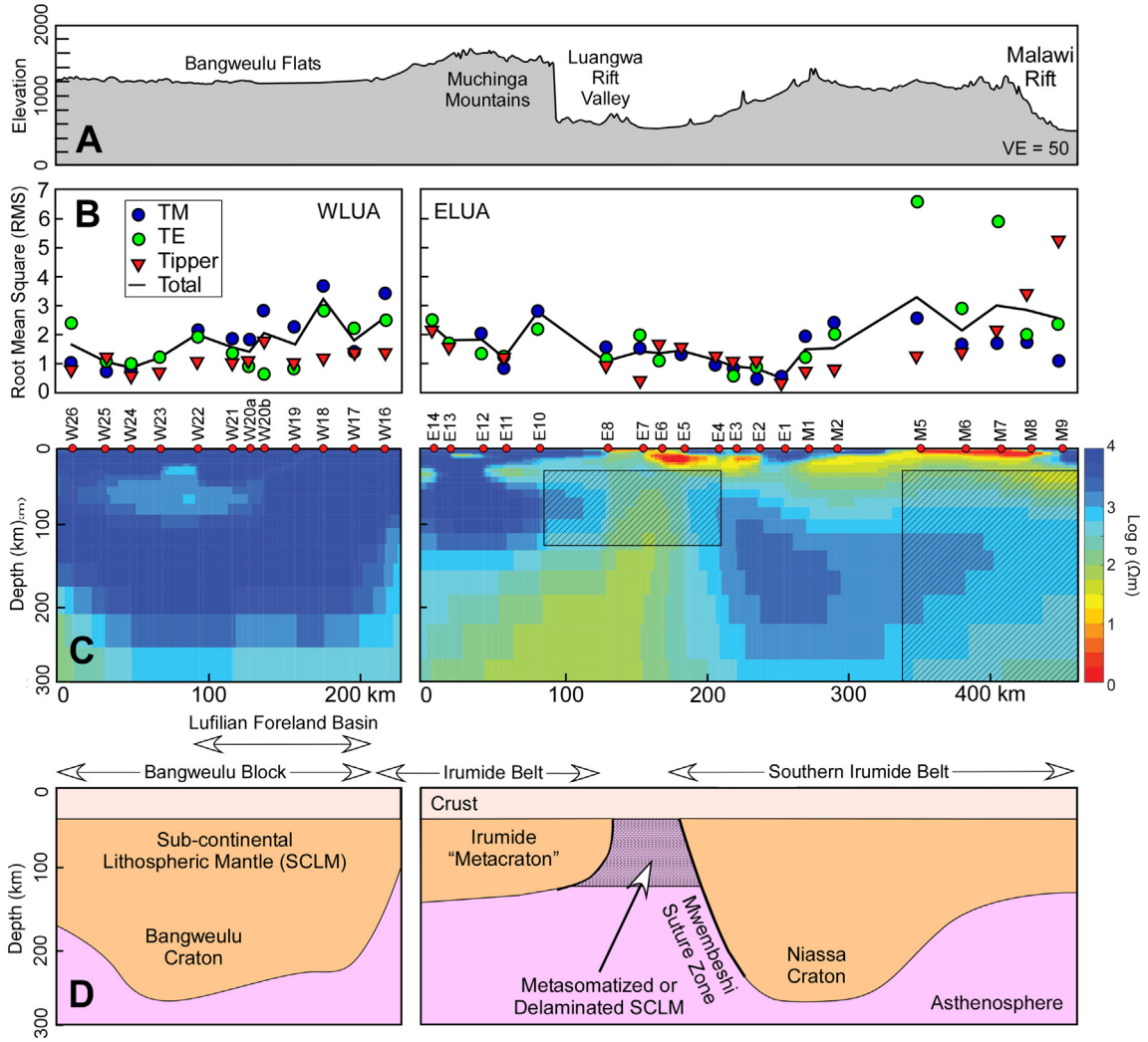

Fig. 6. (A) Topographic profile extracted from Shuttle Radar Topography Mission (SRTM) Digital Elevation Model (DEM) courtesy NASA/JPL-Caltech along the same trace of MT stations. (B) The TE and TM mode, tipper, and total root-mean-squared (RMS) misfit for each station. (C) The preferred 2D isotropic resistivity models for the West Luangwa (WLUA) and East Luangwa (ELUA) profiles with station locations. Warm colors indicate less resistive (more conductive) regions and cool colors indicate more resistive regions. Shaded regions indicate areas of lower resolution in our model. (D) Our interpretation of the upper mantle structure beneath the WLUA and ELUA profiles based on MT and aeromagnetic observations. (For interpretation of the references to colour in this figure legend, the reader is referred to the web version of this article.)

(1) Manually editing the depth of high resistivity in the Irumide Belt mantle.

Increasing the depth of the SCLM of the Irumide Belt to 200 km resulted in poor fit to the observed TM phases (>6°) at the longest periods for sites E14 to E10. The TE phases were not sensitive to the change in resistivity (Fig. S7). The preferred model TE and TM fit phases at all periods generally within 3° (Fig. S6). The systematic misfit in the TM phases, particularly for site E10, shows that a dipping conductive feature beneath the Irumide Belt is required by data.

(2) Increasing crust and upper mantle resistivities between the Irumide and Southern Irumide Belts.

The high conductivities found in the crust beneath sites E5–E8 provide an electromagnetic shielding effect resulting in poor resolution for the underlying mantle structure. Therefore, it is difficult to test if the broad conducting feature beneath sites E6–E8 is a required structural feature or simply a result of spatial smoothing of crustal conductivities during inversion. In order to test data sensitivity to such feature, we increased the lower crust and upper mantle resistivities to smooth the resistivities between sites E4 and E10 (shown by the shaded block in Fig. 6C, right). The TE and TM phase misfit for site E10 increased over all periods (>6°) as a consequence of the higher resistivities. The phases for sites E6–E8 are less sensitive to the change, with only a slight increase in TM phase misfit for the longest periods (Fig. S8). The preferred model TE and TM fit phases at all periods generally within 5° (Fig. S6). These observations might suggest that the upper mantle beneath sites E6–E8 could be more resistive than modeled. However, the high phase difference between the forward response and the observed data at site E10, in addition to the high misfit associated with increasing the mantle resistivity from test (1), show that the manually edited model lacks a dipping conductive feature required by the data. Therefore, the sites directly above the highly conductive crust are not the only constraints for the dipping conductive feature observed. It should be remembered that MT data are approximately as sensitive laterally as they are in depth, i.e., for a uniform Earth the sensitivity would be a hemisphere of radius equal to the depth of penetration. This prompted further sensitivity tests of this feature, including extensive inverse modeling with high tau smoothness values to produce the smoothest

acceptable model possible, and inversions with high horizontal smoothing (alpha) to ensure that vertical smearing of the crustal conductor (to minimize vertical roughness) is not a contributor to the observed structure. We also conducted inversions that solved for the model closest to the starting model after manually increasing the lithospheric resistivities beneath sites E4–10, i.e., the objective function comprised two parts, a part describing the fit of the model responses to the data and a part describing the distance between the new model and the defined prior start model. This contrasts with all our other inversions where the second part of the objective function is a measure of model roughness. The dipping conductive feature was present in the final models of all additional sensitivity tests. We therefore conclude that a region of dipping moderate conductivity most likely extends throughout the entire mantle between the Irumide and Southern Irumide Belts.

(3) Decreasing the depth of high resistivities beneath the Southern Irumide Belt.

Thinning the resistive root beneath the Southern Irumide Belt at sites M2–E5 to 150 km resulted in poor fit to the TM phases (>7°) at the longest periods in sites E2–E4 (Fig. S9). The preferred model TE and TM fit phases at all periods generally within 5° in the region (Fig. S6). The systematic misfit, particularly in the TM phases, indicates that the imaged resistive root is required by the MT data.

(4) Increasing crustal resistivities within Malawi.

Forcing higher crustal resistivities at the eastern end of the profile worsened the misfit to the TE and TM phases at all periods (>10°) for sites M5–M9 (Fig. S10). The preferred model TE and TM fit phases at all periods generally within 3° in the region (Fig. S6). Therefore, the high conductivity upper crust is a robust feature in the model. Resistivities of the mantle beneath sites M5–M9 are poorly constrained due to electromagnetic shielding of the conductive crust (Jones, 1999) and poor data quality due to cultural noise. This area is indicated on the model of Fig. 6C (right) by a shaded block.

Subsequent inversions of each test for WLUA and ELUA removed the manual edits to each feature. Our sensitivity testing shows that all features in the WLUA and ELUA electrical conductivity models are supported by the data.

7. Discussion

7.1. Western Luangwa (WLUA) profile Precambrian lithospheric structure

Based on geological maps of the region, the WLUA profile traverses southeast from the border between Zambia and the Democratic Republic of Congo towards the Luangwa Rift Valley, with most of the profile crossing the Bangweulu Block and the remainder over the southeastern portion of the block that is overlain by the sedimentary rocks of the Lufilian Foreland Basin (Fig. 1B). O'Donnell et al. (2013) found that at a depth of 68 km, the Bangweulu Block is seismically fast (V_S > 4.6 km s^{-1}) with slower shear velocities (V_S ~ 4.4–4.5 km s^{-1}) beneath the Lufilian Foreland Basin. In the O'Donnell et al. (2013) model, the fast shear velocity anomaly migrates SE with increasing depth until 140 km where shear wave speeds start to decrease to ~4.5 km s^{-1}. Based on these observations, O'Donnell et al. (2013) concluded that the lithosphere of the Bangweulu Block extends to a depth of 100 km in this region.

Our electrical model agrees well with the observed seismic structure, but provides a more detailed view of the Precambrian lithospheric structures (Fig. 6C and D). The majority of the profile shows a thick highly resistive block that reaches a maximum thickness of ~250 km in the geographical extent of the Bangweulu Block. The resistivities of this feature range from 100 Ω m to well over 10,000 Ω m requiring an anhydrous, cold mantle. The only possible interpretation of our results is that the Bangweulu Block SCLM is significantly thicker than 100 km in this region and reaches lithospheric thicknesses rivaling that of the Tanzania Craton (Adams et al., 2012; O'Donnell et al., 2013, 140–200 km), the Kaapvaal Craton (Muller et al., 2009, ~200 km; Evans et al., 2011, ~230 km), and the Zimbabwe Craton (Miensopust et al., 2011, ~220 km).

Such thick SCLM supports the interpretation that the Bangweulu Block is a cratonic fragment. The fact that the lithosphere remains thick throughout the WLUA profile, even within the Lufilian Foreland Basin, indicates that the Lufilian is a sedimentary cover over the southeastern edge of the Bangweulu Block.

7.2. Eastern Luangwa (ELUA) profile Precambrian lithospheric structure

The ELUA profile extends from the Irumide Belt in the NW, over the Luangwa Rift Valley and Mwembeshi Shear Zone, and into the Southern Irumide Belt ending at the western edge of the Malawi Rift (Fig. 1B). The shear wave velocity at 68 km depth in the O'Donnell et al. (2013) model for this region is slow (V_S ~ 4.4–4.5 km s^{-1}) relative to the Bangweulu Block to the NW. Velocity increases at greater depths within Zambia until ~200 km, but remains relatively slow near the southern end of the Malawi Rift. This structure is interpreted to be a subsurface extension of the Bangweulu Block into eastern Zambia between 100 and 200 km depth (O'Donnell et al., 2013).

The ~150 km thick resistive feature in the western end of the ELUA profile (Fig. 6C, right) lies within the Irumide Belt. Resistivities of this feature range from ~80 Ω m to over 10,000 Ω m, but are generally >5000 Ω m indicative of cold, anhydrous SCLM. This lithospheric thickness is typical for orogenic belts (Khoza et al., 2013; Miensopust et al., 2011; Muller et al., 2009), which, taken by itself, supports the notion that the Irumide Belt formed entirely during the Irumide Orogeny of the late Mesoproterozoic – Neoproterozoic age. However, U-Pb geochronology on detrital zircons from the Irumide Belt shows that it is primarily Paleoproterozoic in age with signatures of Neoarchean crust components, similar to the Bangweulu Block (De Waele et al., 2009). In fact, geochronological evidence suggests that the Bangweulu Block was once a larger craton, but multiple metacratonization events along its southern margin diminished its size and formed the Irumide Belt (De Waele et al., 2009; De Waele et al., 2006a; De Waele et al., 2006b). With this in mind, the Irumide Belt may have had thicker cratonic lithosphere at one time, but partially lost its lithosphere potentially through delamination (Liégeois et al., 2013) resulting in the lithospheric structure observed in our resistivity model. Based on this interpretation, we identify the resistive feature in the western part of ELUA to be the Irumide Metacraton (Fig. 6D), as suggested in previous studies (De Waele et al., 2006b).

Just east of the Irumide Metacraton is a broad, moderately conductive feature of ~80 Ω m dipping to the west beneath the Irumide Belt that persists throughout the lithosphere and into the asthenosphere. The near surface crust above the feature is highly conductive (~1 Ω m). Similar crustal conductors have been observed along shear and suture zones. This feature coincides with the Mwembeshi Shear Zone and Luangwa Rift Valley that separates the Irumide and Southern Irumide Belts (Westerhof et al., 2008). The Mwembeshi Shear Zone has a distinct magnetic fabric (ductile NE-trending fabric) that is easily recognized on the vertical and tilt derivative maps and underlies stations E5–E7. These near surface conductive anomalies are generally interpreted as graphite and sulfides that experienced shear and metamorphism, such as during subduction (Bouzid et al., 2015; Jones et al., 2005; Wannamaker, 2005; Yang et al., 2015). The extent of the Mwembeshi Shear Zone into the mantle (Fig. 6C and D) has never before been imaged, but similar mantle features have been observed in regions of ancient subduction zones (Yang et al., 2015) and ancient fault zones (Jones and Garcia, 2006). Our electrical conductivity model

testing shows that the resistivity of the upper mantle directly beneath the near surface conductivity anomaly is less well-resolved (indicated by the hatched box on Fig. 6C, right). However, the longer periods of sites to the west (E10 to E14) require the dipping conductive feature at greater depths beneath the Irumide Metacraton. Therefore, based on our electrical conductivity model testing, the shear zone extends throughout the mantle and separates the lithosphere of the Irumide Metacraton from the lithosphere of the Southern Irumide Belt and most likely represents a suture zone. This interpretation is further supported by the variations in magnetic fabric observed in the aeromagnetic data over the Mwembeshi Shear Zone (Fig. 3). The suture zone most likely formed during the Irumide Orogeny in the Mesoproterozoic when the two lithospheric fragments collided as the oceanic slab subducted beneath the Irumide Belt (Johnson et al., 2006; Johnson et al., 2007). The higher conductivity of the mantle in this feature may be due to conductive phases, such as carbon or sulfides, being carried to great depths during subduction (Yang et al., 2015), or as a result of mineral shearing (Pommier et al., 2015) during subduction in the Irumide Orogeny or during reworking in the Damara-Lufilian-Zambezi Orogeny. The presence of such a strong lithospheric discontinuity may have facilitated the percolation of fluids into the lithosphere resulting in metasomatization and assisting the delamination of the SCLM beneath the Irumide Belt, forming the Irumide Metacraton (Liégeois et al., 2013).

It has been suggested that the development of the Luangwa Rift during the Paleozoic – Mesozoic was largely controlled by the Mwembeshi Shear Zone (Daly et al., 1989; Orpen et al., 1989; Banks et al., 1995). Recent seismic surveys observe seismic activity and slower seismic velocities at depth within the Luangwa Rift Valley, but seismic resolution is limited in our study region (e.g., Craig et al., 2011; O'Donnell et al., 2013 and references therein). It is possible that this rifting event has further enhanced the electrical conductivity anomaly that we observed beneath the Mwembeshi Shear Zone. However, we are uncertain about the level of contribution of the Luangwa Rift to this anomaly since it is an amagmatic rift.

The Southern Irumide Belt is covered by the central portion of the ELUA profile (Fig. 1B). The electrical conductivity model shows a more conductive crust (resistivities as low as 1 Ω m) of ~40 km thickness than found within the Irumide Metacraton. Beneath the crust is a highly resistive anomaly ranging from 100 Ω m to several 1000 Ω m that persists to depths of 250 km (Fig. 6C and D). As previously discussed, the Southern Irumide Belt is thought to have a cratonic nucleus that is "lost" beneath the surface sedimentary cover and episodes of rifting (Andreoli, 1984). The resistive anomaly observed in our electrical conductivity model is similar in thickness to the Bangweulu Block in the northwest. The observed resistivity and thickness most likely represents a cold, anhydrous cratonic SCLM. A seismically fast shear wave feature was identified at approximately the same depths in southeastern Zambia as our resistive anomaly, and was interpreted to be a southern subsurface continuation of the Bangweulu Block (O'Donnell et al., 2013). However, our conductivity model clearly shows a suture zone between the Irumide Metacraton and Southern Irumide Belt. We therefore believe that this resistive anomaly is a cratonic block separate from the Bangweulu Block and identify it to be the Niassa Craton. Arcuate shaped magnetic fabrics beneath stations E4–E1 on the vertical and tilt derivative maps are coincident with the edges of this craton at depth (Fig. 3). This interpretation does not match seismic results as well as for the WLUA profile, which may be a resolution issue. O'Donnell et al. (2013) greatly refined the Zambian lithospheric structures, but still focused on a broad area around the Tanzania Craton. Resolution tests of their data showed that, at the depths of interest, features in eastern Zambia are significantly smeared. Therefore, as a result of the extent of their study region the seismic model may have smoothed the Niassa Craton such that it remained indistinguishable from the lithosphere of the Irumide and Bangweulu Block to the northwest.

In Malawi, the electrical model shows a very conductive shallow crust with resistivities around 1 Ω m (Fig. 6C and D). Resistivities of the mantle below this feature cannot be resolved due to electromagnetic shielding and are instead defined by vertical smoothing during inversion (Jones, 1999). The lower resistivities near the Malawi Rift are in agreement with the slower shear wave velocity observed in seismic results (Accardo et al., 2017; O'Donnell et al., 2013; O'Donnell et al., 2016), and may be related to rifting in the Western Branch of the EARS producing a much warmer lithosphere. However, our model misfit to particularly the TE mode responses is highest in this region suggesting that resolution is limited.

The crustal layer continues throughout much of the ELUA model, but particularly the Mwembeshi Suture Zone, Southern Irumide Belt (Niassa Craton), and Malawi Rift are characterized by sub-horizontal layers of conductive anomalies. It is possible that these represent fluids exploiting crustal scale detachment faults. This is in good agreement with Johnson et al. (2006, 2007) who suggested that the Southern Irumide is composed of allochthonous continental margin terranes assembled during the Irumide Orogeny.

8. Conclusions

We have employed analysis and modeling of deep-probing magnetotelluric (MT) data and aeromagnetic data to gain insight into the lithospheric structure of the Precambrian entities of eastern Zambia and southern Malawi, which include the Archean-Paleoproterozoic cratonic Bangweulu Block, the Mesoproterozoic-Neoproterozoic Irumide and Southern Irumide Orogenic Belts, and the Lufilian Foreland Basin. We find that the lithosphere beneath the Bangweulu Block is highly resistive to a depth of order 250 km, consistent with lithospheric thicknesses of other cratonic blocks in southern Africa and worldwide. In contrast, the Irumide Belt lithosphere reaches a depth of 150–180 km, typical of orogenic belts throughout southern Africa. The Irumide Belt is not as resistive as the Bangweulu Block, suggesting partial SCLM modification. Using published geochronological data as constraints, we interpret the observed MT structure beneath the Irumide Belt as thinning of a cratonic SCLM, possibly through partial delamination by the Mwembeshi Shear Zone that is clearly identifiable by its distinct magnetic fabric. We propose to rename the Irumide Orogenic Belt the Irumide Metacraton following the suggestion of De Waele et al. (2006b) that the Irumide Belt is the metacratonic boundary of the Bangweulu Block. We find moderately resistive lithosphere beneath the Southern Irumide Belt extending to a depth of 250 km. This corroborates the inferred presence of the Niassa Craton - a cratonic nucleus inferred from early surface geology studies. We find sub-horizontal layers of conductive anomalies in the crust of the Southern Irumide Belt and we interpret these as crustal-scale detachments, possibly due to the thrust of the Southern Irumide Belt on top of Niassa Craton. In addition, our models reveal a broad mantle discontinuity at the boundaries between the Irumide Metacraton and the Niassa Craton. We interpret this as SCLM modification along a lithospheric suture zone as a result of ancient subduction.

Acknowledgements

We thank J-P Liegeois and K. Selway for their detailed and constructive reviews. Funding for this research was provided by the National Science Foundation, grant number EAR-1010432 through the Continental Dynamics Program and EAR-1255233. The results presented in this paper rely on data collected at magnetic observatories. We thank the national institutes that support them and INTERMAGNET for promoting high standards of magnetic observatory practice (www.intermagnet.org). The aeromagnetic data used in this study can be obtained from the Geological Survey Department of Zambia. We thank Richard Sullivan, Trevor Harrison for MT instrument deployment, and the Geological Survey Department of Zambia for MT instrument deployment and aeromagnetic data collection. This is Oklahoma State University Boone Pickens School of Geology contribution #2017-75.

Appendix A. Supplementary data

Supplementary data to this article can be found online at https://doi.org/10.1016/j.gr.2017.09.007.

References

Abdelsalam, M.G., Liégeois, J.-P., Stern, R.J., 2002. The Saharan metacraton. Journal of African Earth Sciences 34, 119–136.

Abdelsalam, M.G., Gao, S.S., Liégeois, J.-P., 2011. Upper mantle structure of the Saharan metacraton. Journal of African Earth Sciences 60, 328–336.

Accardo, N.J., Gaherty, J.B., Shillington, D.J., Ebinger, C.J., Nyblade, A.A., Mbogoni, G.J., Chindandali, P.R.N., Ferdinand, R.W., Mulibo, G.D., Kamihanda, G., Keir, D., Scholz, C., Selway, K., O'Donnell, J.P., Tepp, G., Gallacher, R., Mtelela, K., Mruma, A., 2017. Surface wave imaging of the weakly extended Malawi Rift from ambient-noise and teleseismic Rayleigh waves from onshore and lake-bottom seismometers. Geophysical Journal International 209 (3), 1892–1905.

Ackermann, E., 1950. Ein neuer Faltengürtel in Nordrhodesien und seine tektonische Stellung im afrikanischen Grundgebirge. Geologische Rundschau 38, 24–39.

Ackermann, E., 1960. Strukturen im Untergrund eines interkratonischen Doppel-Orogens (Irumiden, Nordrhodesien). Geologische Rundschau 50, 538–553.

Adams, A., Nyblade, A., Weeraratne, D., 2012. Upper mantle shear wave velocity structure beneath the East African plateau: evidence for a deep, plateauwide low velocity anomaly. Geophysical Journal International 189, 123–142.

Andersen, L., Unrug, R., 1984. Geodynamic evolution of the Bangweulu Block, northern Zambia. Precambrian Research 25, 187–212.

Andreoli, M.A.G., 1984. Petrochemistry, tectonic evolution and metasomatic mineralisations of Mozambique belt granulites from S. Malawi and Tete (Mozambique). Precambrian Research 25, 161–186.

Arndt, N., Coltice, N., Helmstaedt, H., Gregoire, M., 2009. Origin of Archean subcontinental lithospheric mantle: some petrological constraints. Lithos 109, 61–71.

Artemieva, I.M., Mooney, W.D., 2001. Thermal thickness and evolution of Precambrian lithosphere: a global study. Journal of Geophysical Research: Solid Earth 106, 16387–16414.

Banks, N., Bardwell, K., Musiwa, S., 1995. Karoo rift basins of the Luangwa valley, Zambia. Geological Society of London Special Publications 80, 285–295.

Batumike, M.J., Kampunzu, A.B., Cailteaux, J.H., 2006. Petrology and geochemistry of the Neoproterozoic Nguba and Kundelungu Ggroup, Katangan Supergroup, southeast Congo – implication for province, paleoweathering and geotectonic setting. Journal of African Earth Sciences 44, 97–115.

Begg, G., Griffin, W., Natapov, L., O'Reilly, S.Y., Grand, S., O'Neill, C., Hronsky, J., Djomani, Y.P., Swain, C., Deen, T., 2009. The lithospheric architecture of Africa: seismic tomography, mantle petrology, and tectonic evolution. Geosphere 5, 23–50.

Black, R., Liégeois, J.-P., 1993. Cratons, mobile belts, alkaline rocks and continental lithospheric mantle: the Pan-African testimony. Journal of the Geological Society, London 150, 89–98.

Boniface, N., Schenk, V., 2012. Neoproterozoic eclogites in the Paleoproterozoic Ubendian Belt of Tanzania: evidence for a Pan-African suture between the Bangweulu Block and the Tanzania Craton. Precambrian Research 208, 72–89.

Bouzid, A., Bayou, B., Liégeois, J.-P., Bourouis, S., Bougchiche, S.S., Bendekken, A., Abtout, A., Boukhlouf, W., Ouabadi, A., 2015. Lithospheric structure of the Atakor metacratonic volcanic swell (Hoggar, Tuareg Shield, southern Algeria): electrical constraints from magnetotelluric data. Geological Society of America Special Papers 514, SPE514–515.

Cailteux, J.L.H., Kampunzu, A.B., Batumike, M.J., 2005. Lithostratigraphic position and petrographic characteristics of R.A.T. ("Roches Argilo-Talqueuses") Subgroup, Neoproterozoic Katangan Belt (Congo). Journal of African Earth Sciences 42, 82–94.

Caldwell, T.G., Bibby, H.M., Brown, C., 2004. The magnetotelluric phase tensor. Geophysical Journal International 158, 457–469.

Craig, T.J., Jackson, J.A., Priestley, K., McKenzie, D., 2011. Earthquake distribution patterns in Africa: their relationship to variations in lithospheric and geological structure, and their rheological implications. Geophysical Journal International 185, 403–434.

Daly, M., 1986. The intracratonic Irumide belt of Zambia and its bearing on collision orogeny during the Proterozoic of Africa. Geological Society, London, Special Publications 19, 321–328.

Daly, M., Chorowicz, J., Fairhead, J., 1989. Rift basin evolution in Africa: the influence of reactivated steep basement shear zones. Geological Society of London Special Publications 44, 309–334.

De Waele, B., Wingate, M.T., Fitzsimons, I.C., Mapani, B.S., 2003. Untying the Kibaran knot: a reassessment of Mesoproterozoic correlations in southern Africa based on SHRIMP U-Pb data from the Irumide belt. Geology 31, 509–512.

De Waele, B., Kampunzu, A., Mapani, B., Tembo, F., 2006a. The Mesoproterozoic Irumide belt of Zambia. Journal of African Earth Sciences 46, 36–70.

De Waele, B., Liégeois, J.-P., Nemchin, A.A., Tembo, F., 2006b. Isotopic and geochemical evidence of Proterozoic episodic crustal reworking within the Irumide Belt of south-central Africa, the southern metacratonic boundary of an Archaean Bangweulu Craton. Precambrian Research 148, 225–256.

De Waele, B., Fitzsimons, I., Wingate, M., Tembo, F., Mapani, B., Belousova, E., 2009. The geochronological framework of the Irumide Belt: a prolonged crustal history along the margin of the Bangweulu Ccraton. American Journal of Science 309, 132–187.

Deen, T.J., Griffin, W., Begg, G., O'Reilly, S.Y., Natapov, L., Hronsky, J., 2006. Thermal and compositional structure of the subcontinental lithospheric mantle: derivation from shear wave seismic tomography. Geochemistry, Geophysics, Geosystems 7.

Evans, R.L., Jones, A.G., Garcia, X., Muller, M., Hamilton, M., Evans, S., Fourie, C.J.S., Spratt, J., Webb, S., Jelsma, H., Hutchins, D., 2011. Electrical lithosphere beneath the Kaapvaal craton, southern Africa. Journal of Geophysical Research 116.

Griffin, W.L., O'Reilly, S.Y., Alfonso, C., Begg, G.C., 2009. The composition and evolution of lithospheric mantle: a re-evaluation and its tectonic implications. Journal of Petrology 50, 1185–1204.

Groom, R.W., Bailey, R.C., 1989. Decomposition of magnetotelluric impedance tensors in the presence of local three-dimensional galvanic distortion. Journal of Geophysical Research: Solid Earth 94, 1913–1925.

Hirth, G., Evans, R.L., Chave, A.D., 2000. Comparison of continental and oceanic mantle electrical conductivity: is the Archean lithosphere dry? Geochemistry, Geophysics, Geosystems 1.

Irving, E., Irving, G., 1982. Apparent polar wander paths Carboniferous through Cenozoic and the assembly of Gondwana. Geophysical Surveys 5, 141–188.

Johnson, S.P., Rivers, T., De Waele, B., 2005. A review of the Mesoproterozoic to early Palaeozoic magmatic and tectonothermal history of south–central Africa: implications for Rodinia and Gondwana. Journal of the Geological Society 162, 433–450.

Johnson, S., De Waele, B., Liyungu, K., 2006. U-Pb sensitive high-resolution ion microprobe (SHRIMP) zircon geochronology of granitoid rocks in eastern Zambia: terrane subdivision of the Mesoproterozoic southern Irumide Belt. Tectonics 25.

Johnson, S.P., De Waele, B., Tembo, F., Katongo, C., Tani, K., Chang, Q., Iizuka, T., Dunkley, D., 2007. Geochemistry, geochronology and isotopic evolution of the Chewore–Rufunsa Terrane, Southern Irumide Belt: a Mesoproterozoic continental margin arc. Journal of Petrology 48, 1411–1441.

Jones, A.G., 1999. Imaging the continental upper mantle using electromagnetic methods. Lithos 48, 57–80.

Jones, A.G., Garcia, X., 2006. Electrical resistivity structure of the Yellowknife River Fault Zone and surrounding region. Gold in the Yellowknife Greenstone Belt, Northwest Territories: Results of the EXTECH III Multidisciplinary Research Project. Geological Association of Canada, Mineral Deposits Division, Special Publication No. 3, Chapter 10, pp. 126–141.

Jones, A.G., Jödicke, H., 1984. Magnetotelluric transfer function estimation improvement by a coherence-based rejection technique. SEG Technical Program Expanded Abstracts 1984. Society of Exploration Geophysicists, pp. 51–55.

Jones, A.G., Chave, A.D., Egbert, G., Auld, D., Bahr, K., 1989. A comparison of techniques for magnetotelluric response function estimation. Journal of Geophysical Research 94, 14201.

Jones, A.G., Ledo, J., Ferguson, I.J., 2005. Electromagnetic images of the Trans-Hudson orogen: the north American Central Plains anomaly revealed. Canadian Journal of Earth Sciences 42, 457–478.

Kampunzu, A.B., Cailteux, J., 1999. Tectonic evolution of the Lufilian Arc (Central Africa Copper Belt) during Neoproterozoic Pan African Orogenesis. Gondwana Research 2, 401–421.

Katongo, C., Koller, F., Kloetzli, U., Koeberl, C., Tembo, F., De Waele, B., 2004. Petrography, geochemistry, and geochronology of granitoid rocks in the Neoproterozoic-Paleozoic Lufilian–Zambezi belt, Zambia: implications for tectonic setting and regional correlation. Journal of African Earth Sciences 40, 219–244.

Khoza, D., Jones, A., Muller, M., Evans, R., Webb, S., Miensopust, M., 2013. Tectonic model of the Limpopo belt: constraints from magnetotelluric data. Precambrian Research 226, 143–156.

Lebedev, S., Boonen, J., Trampert, J., 2009. Seismic structure of Precambrian lithosphere: new constraints from broad-band surface-wave dispersion. Lithos 109, 96–111.

Lenoir, J.L., Liégeois, J.-P., Theunissen, K., Klerkx, J., 1994. The Palaeoproterozoic Ubendian shear belt in Tanzania: geochronology and structure. Journal of African Earth Sciences 19, 169–184.

Liégeois, J.P., Latouche, L., Boughrara, M., Navez, J., Guiraud, M., 2003. The LATEA metacraton (central Hoggar, Tuareg shield, Algeria): behaviour of an old passive margin during the Pan-African orogeny. Journal of African Earth Sciences 37, 161–190.

Liégeois, J.-P., Abdelsalam, M.G., Ennih, N., Ouabadi, A., 2013. Metacraton: nature, genesis and behavior. Gondwana Research 23, 220–237.

Maruyama, S., Liou, J., 1998. Initiation of ultrahigh-pressure metamorphism and its significance on the Proterozoic–Phanerozoic boundary. Island Arc 7, 6–35.

Master, S., Raiauld, C., Armstrong, R.A., Phillips, D., Robb, L.J., 2005. Province ages of the Neoproterozoic Katanga Supergroup (Central African Copperfield), with implications for basin evolution. Journal of African Earth Sciences 42, 41–60.

McConnell, R., 1972. Geological development of the rift system of eastern Africa. Geological Society of America Bulletin 83, 2549–2572.

McNeice, G.W., Jones, A.G., 2001. Multisite, multifrequency tensor decomposition of magnetotelluric data. Geophysics 66, 158–173.

Miensopust, M.P., Jones, A.G., Muller, M.R., Garcia, X., Evans, R.L., 2011. Lithospheric structures and Precambrian terrane boundaries in northeastern Botswana revealed through magnetotelluric profiling as part of the southern African Magnetotelluric Experiment. Journal of Geophysical Research 116.

Miller, H.G., Singh, V., 1994. Potential field tilt - a new concept for location of potential field sources. Journal of Applied Geophysics 32, 213–217.

Muller, M.R., Jones, A.G., Evans, R.L., Grütter, H.S., Hatton, C., Garcia, X., Hamilton, M.P., Miensopust, M.P., Cole, P., Ngwisanyi, T., Hutchins, D., Fourie, C.J., Jelsma, H.A., Evans, S.F., Aravanis, T., Pettit, W., Webb, S.J., Wasborg, J., 2009. Lithospheric structure, evolution and diamond prospectivity of the Rehoboth Terrane and western Kaapvaal craton, southern Africa: constraints from broadband magnetotellurics. Lithos 112, 93–105.

Nyblade, A.A., Brazier, R.A., 2002. Precambrian lithospheric controls on the development of the East African rift system. Geology 30, 755–758.

O'Donnell, J., Adams, A., Nyblade, A., Mulibo, G., Tugume, F., 2013. The uppermost mantle shear wave velocity structure of eastern Africa from Rayleigh wave tomography: constraints on rift evolution. Geophysical Journal International 194, 961–978.

O'Donnell, J.P., Selway, K., Nyblade, A.A., Brazier, R.A., El Tahir, N., Durrheim, R.J., 2016. Thick lithosphere, deep crustal earthquakes and no melt: a triple challenge to understanding extension in the western branch of the East African Rift. Geophysical Journal International 204, 985–998.
Orpen, J.L., Swain, C.J., Nugent, C., Zhou, P.P., 1989. Wrench-fault and half-graben tectonics in the development of the Palaeozoic Zambezi Karoo Basins in Zimbabwe - the "Lower Zambezi" and "Mid-Zambezi" basins respectively - and regional implications. J. Afr. Earth Sci. 8, 215–229.
Pasyanos, M.E., 2010. Lithospheric thickness modeled from long-period surface wave dispersion. Tectonophysics 481, 38–50.
Pasyanos, M.E., Nyblade, A.A., 2007. A top to bottom lithospheric study of Africa and Arabia. Tectonophysics 444, 27–44.
Peslier, A.H., Woodland, A.B., Bell, D.R., Lazarov, M., 2010. Olivine water contents in the continental lithosphere and the longevity of cratons. Nature 467, 78–81.
Pollack, H.N., 1986. Cratonization and thermal evolution of the mantle. Earth and Planetary Science Letters 80, 175–182.
Pommier, A., Leinenweber, K., Kohlstedt, D.L., Qi, C., Garnero, E.J., Mackwell, S.J., Tyburczy, J.A., 2015. Experimental constraints on the electrical anisotropy of the lithosphere-asthenosphere system. Nature 522, 202–206.
Porada, H., Berhorst, V., 2000. Towards a new understanding of the Neoproterozoic-Early Palaeozoic Lufilian and northern Zambezi Belts in Zambia and the Democratic Republic of Congo. Journal of African Earth Sciences 30, 727–771.
Ritsema, J., van Heijst, H., 2000. New seismic model of the upper mantle beneath Africa. Geology 28, 63–66.
Rodi, W., Mackie, R.L., 2001. Nonlinear conjugate gradients algorithm for 2-D magnetotelluric inversion. Geophysics 66, 174–187.
Rousseeuw, P.J., 1984. Least median of squares regression. Journal of the American Statistical Association 79, 871–880.
Salem, A., Williams, S., Fairhead, D., Smith, R., Ravat, D., 2007. Interpretation of magnetic data using tilt-angle derivatives. Geophysics 73, L1–L10.
Selley, D., Broughton, D., Scott, R., Hitzman, M., Bull, S.W., large, R.R., McGoldrick, P.J., Croaker, Mawson, Pollington, N., Barra, F., 2005. A new look at the geology of the Zambian Copperfield. In: Hedenquist, J.W., Thompson, J.F.H., Goldfarb, R.J., Richards, J.P. (Eds.), Economic Geology – One Hundredth Anniversary. Vols. 1905-2005. Society of Economic Geologists, Littleon, Colp, pp. 965–1000.
Selway, K., 2015. Negligible effect of hydrogen content on plate strength in East Africa. Nature Geoscience 8, 543–546.
Shapiro, N., Ritzwoller, M., 2002. Monte-Carlo inversion for a global shear-velocity model of the crust and upper mantle. Geophysical Journal International 151, 88–105.
Smith, A.G. and Hallam, A. (1970) The fit of the southern continents.
Smith, R.S., Salem, A., 2005. Imaging depth, structure, and susceptibility from magnetic data: the advanced source-parameter imaging method. Geophysics 70, L31–L38.
Stern, R.J., 2008. Neoproterozoic crustal growth: the solid Earth system during a critical episode of Earth history. Gondwana Research 14, 33–50.
Thébault, E., Finlay, C.C., Beggan, C.D., Alken, P., Aubert, J., Barrois, O., Bertrand, F., Bondar, T., Boness, A., Brocco, L., Canet, E., Chambodut, A., Chulliat, A., Coïsson, P., Civet, F., Du, A., Fournier, A., Fratter, I., Gillet, N., Hamilton, B., Hamoudi, M., Hulot, G., Jager, T., Korte, M., Kuang, W., Lalanne, X., Langlais, B., Léger, J., Lesur, V., Lowes, F.J., et al., 2015. International geomagnetic reference field: the 12th generation. Earth, Planets and Space 2015 (67), 79.
Thurston, J.B., Smith, R.S., 1997. Automatic conversion of magnetic data to depth, dip, and susceptibility contrast using the SPI (TM) method. Geophysics 62, 807–813.
Verduzco, B., Fairhead, J.D., Green, C.M., MacKenzie, C., 2004. New insights into magnetic derivatives for structural mapping. The Leading Edge 23, 116–119.
Wannamaker, P.E., 2005. Anisotropy versus heterogeneity in continental solid earth electromagnetic studies: fundamental response characteristics and implications for physicochemical state. Surveys in Geophysics 26, 733–765.
Westerhof, A.P., Lehtonen, M.I., Mäkitie, H., Manninen, T., Pekkala, Y., Gustafsson, B., Tahon, A., 2008. The Tete-Chipata Belt: a new multiple terrane element from western Mozambique and southern Zambia. Geological Survey of Finland Special Paper 48, 145–166.
Yang, B., Egbert, G.D., Kelbert, A., Meqbel, N.M., 2015. Three-dimensional electrical resistivity of the north-central USA from EarthScope long period magnetotelluric data. Earth and Planetary Science Letters 422, 87–93.
Zientek, M.L., Bliss, J.D., Broughton, D.W., Christie, M., Denning, P.D., Hayes, T.S., Hizman, M.W., Horton, J.D., Frost-Killian, S., Jack, D.J., Master, S., Parks, H.L., Taylor, C.D., Wilson, A.B., Wintzer, N.E., Woodhear, J., 2014. Sediment-hosted stratabound copper assessment of the Neoproterozoic Roan Group, Central African Copperbelt, Katanga Basin, Democratic Republic of Congo and Zambia. U.S. Geological Survey Scientific Investigations Report 2010-5090-T, 162 p. and Spatial Data https://doi.org/10.3133/sir20110509OT.